Popular summary

Retrieval of cloud pressure and chlorophyll content using Raman scattering in GOME ultraviolet spectra

Joanna Joiner, Alexander Vasilkov, David Flittner, James Gleason, P. K. Bhartia

When incoming solar light interacts with air molecules in the atmosphere and water molecules in the ocean, most of the scattered light has the same wavelength as the incoming light. For example, ultraviolet incoming radiation will be scattered and will remain mostly as ultraviolet light. This is called Rayleigh scattering. However, a small fraction of the scattered light is shifted towards either redder or bluer wavelengths. This is known as Raman scattering. Raman scattering produces an interesting effect when ultraviolet observations from satellites are made at different wavelengths. Wavy features appear in solar spectrum due to absorption of radiation by elements in the sun like Calcium. When the backscattered light is observed by a satellite, the wavy structures appear to be slightly smeared.

Clouds can reflect a large amount of incoming sunlight back to space or to a satellite. The clouds can act as a blocker to prevent light from reaching the ground and atmosphere below the cloud. This causes a decrease in Rayleigh and Raman scattering. The higher the cloud, the bigger the blocking effect is. By measuring the amount of spectral smearing and using sophisticated models to estimate the magnitude of the smearing for different conditions, we can infer how high a cloud is. A similar effect occurs in the ocean, except that instead of clouds, living organisms and dissolved organic matter in the water act as light blockers.

For the first time, we have used the smearing effect to retrieve concentrations of chlorophyll in the ocean. The results compare well with other remote sensing techniques. Our approach has the advantage that it is less sensitive to absolute calibration errors and other types of atmospheric interference. It is also complementary to other approaches in that it has very high sensitivity in relatively clear waters with little chlorophyll.

We have also demonstrated that our technique can be used to retrieve cloud pressures with more sophisticated and accurate instruments than were used previously. We plan to use this approach to determine cloud pressure with an instrument that will fly on NASA's Earth Observing System Aura satellite. It is important to know how high clouds are in order to accurately retrieve information about ozone and other pollutants in the troposphere.

Retrieval of cloud pressure and chlorophyll content using Raman scattering in GOME ultraviolet spectra

Joanna Joiner[1]

Alexander P. Vasilkov[2]

David E. Flittner[3]

James F. Gleason[1]

Pawan K. Bhartia[1]

[1]Laboratory for Atmospheres, NASA Goddard Space Flight Center, Greenbelt, Maryland, USA

[2]Science Systems and Applications Inc., Lanham, Maryland, USA

[3]University of Arizona, Tucson, Arizona, USA

P. K. Bhartia and J. F. Gleason, NASA Goddard Space Flight Center, Code 916, Greenbelt, MD 20771 USA. (e-mail:bhartia@carioca.gsfc.nasa.gov, gleason@redwind.gsfc.nasa.gov)

D. E. Flittner, Cooperative Center for Atmospheric Science and Technology (CCAST), University of Arizona Tucson, AZ 85721, USA. (e-mail:flittner@jet.atmo.arizona.edu)

J. Joiner, NASA Goddard Space Flight Center, Code 910.3, Greenbelt, MD 20771, USA. (e-mail:joiner@dao.gsfc.nasa.gov)

A. P. Vasilkov, Science Systems and Applications Inc., 10210 Greenbelt, Rd., Ste 400, Lanham, MD 20706, USA. (e-mail:alexander_vassilkov@sesda.com)

Abstract.

Reliable cloud pressure estimates are needed for accurate retrieval of ozone and other trace gases using satellite-borne backscatter ultraviolet (buv) instruments such as the global ozone monitoring experiment (GOME). Cloud pressure can be derived from buv instruments by utilizing the properties of rotational-Raman scattering (RRS) and absorption by O_2-O_2. In this paper we estimate cloud pressure from GOME observations in the 355-400 nm spectral range using the concept of a Lambertian-equivalent reflectivity (LER) surface. GOME has full spectral coverage in this range at relatively high spectral resolution with a very high signal-to-noise ratio. This allows for much more accurate estimates of cloud pressure than were possible with its predecessors SBUV and TOMS. We also demonstrate the potential capability to retrieve chlorophyll content with full-spectral buv instruments.

We compare our retrieved LER cloud pressure with cloud top pressures derived from the infrared ATSR instrument on the same satellite. The findings confirm results from previous studies that showed retrieved LER cloud pressures from buv observations are systematically higher than IR-derived cloud-top pressure. Simulations using Mie-scattering radiative transfer algorithms that include O_2-O_2 absorption and RRS show that these differences can be explained by increased photon path length within and below cloud.

1. Introduction

Observations of cloud properties, such as cloud-top pressure, are important for understanding the Earth's radiation budget as well as for validating general circulation model simulations [*e.g., Ramanathan, 1987*] and for data assimilation. Accurate cloud pressures are also needed for a variety of remote sensing problems including trace gas retrievals.

Thermal infrared satellite data have traditionally been used to estimate cloud-top pressure for cloud climatological data sets [*e.g., Rossow and Schiffer, 1991*]. Other methods based on absorption in the oxygen A band [*e.g., Koelemeijer et al., 2001*] and rotational-Raman scattering (RRS) [*Joiner and Bhartia*, 1995] (JB95) have also been developed to estimate cloud pressure from satellite-borne instruments.

JB95 derived effective UV cloud pressures using RRS with the Nimbus-7 Total Ozone Mapping Spectrometer (TOMS) and Solar Backscatter Ultraviolet (SBUV) radiometer continuous spectral scan observations. RRS produces filling-in and depletion of solar Fraunhofer lines in Earth backscattered spectra at ultraviolet wavelengths [*e.g., Kattawar et al.*, 1982; *Joiner et al.*, 1995; Chance and Spurr, 1997]. This filling-in is known as the Ring effect [*Grainger and Ring*, 1962] and its inclusion in satellite retrievals of trace gases is important [*e.g., Vountas et al.*, 1998].

JB95 derived reasonable cloud pressures with TOMS and SBUV despite several limitations including the relatively low signal-to-noise ratio of TOMS and large pixel size (200 km) of SBUV. UV cloud pressures were systematically higher than those from the coincident Nimbus-7 temperature-humidity infrared radiometer (THIR). This difference was explained by the fact that the Lambert-equivalent reflectivity (LER) pressure retrieved using UV observations is an effective pressure that would be observed if the cloud had

Lambertian properties. Scattering within and beneath the cloud effectively increases the retrieved LER pressure to a value greater than that of the physical cloud top.

Enhanced RRS in a cloudy atmosphere was simulated in a radiative transfer model (SCIATRAN) with Mie scattering using semi-infinite layers or an effective reflecting boundary [*e.g., de Beek et al.*, 2001 and references therein]. They compared their model results with satellite data from the Global Ozone Monitoring Experiment (GOME) and ground-based measurements at wavelengths between 390 and 400 nm where filling-in of the solar Fraunhofer Ca lines occurs. Their results showed good agreement between model and measurements where local conditions could be estimated with reasonable accuracy. They showed that the filling-in depends on cloud optical thickness (COT) when COTs are below about 50. At COTs above 50, the filling-in saturates and the dependence on cloud top pressure is similar to that of the LER shown in JB95.

Understanding Raman and Rayleigh scattering in a cloudy atmosphere is important for the interpretation of data from instruments such as TOMS, SBUV, and GOME. These instruments are a primary data source used to produce global climatologies and estimate trends of ozone and other trace gases [*e.g., Stolarski et al.*, 1992; *Gleason et al.*, 1993; *McPeters et al.*, 1996; *Burrows et al.*, 1999]. Errors in the assumed cloud pressure can produce non-negligible errors in retrieved total column ozone [*Koelemeijer and Stammes*, 1999] from buv instruments. It has also been shown that using infrared-derived cloud pressures and climatologies can produce errors in retrieved total column ozone [*e.g., Thompson et al.*, 1993, *Hsu et al.*, 1997] and tropospheric ozone [*Hudson et al.*, 1995].

Cloud pressures are needed to study long term and seasonal variations in tropical tropospheric ozone derived from cloud slicing techniques [*e.g., Chandra et al.*, 1998,1999;

Ziemke and Chandra, 1999]. *Ziemke et al.* [1999] derived total troposperic column ozone (TCO) without a direct cloud measurement in the tropics by assuming that deep convective clouds reach the tropopause. *Ziemke et al.*, [2001] combined TCO from this method with upper tropospheric ozone derived from cloud slicing using cloud pressures from the Nimbus 7 temperature-humidity and infrared radiometer (THIR) to estimate the lower tropospheric ozone. If a direct and appropriate cloud pressure were available, the cloud slicing technique could perhaps be applied more accurately and extended to other latitudes.

In this study we extend the spectral range and coverage of the previous studies to retrieve cloud pressure using GOME observations between 355 and 400 nm. Within this wavelength region there are two O_2-O_2 absorption lines. RRS affects observations throughout this spectral region. Absorption from O_3 and other trace gases is very small. The approach used here has added several new elements to the basic concept of JB95.

Vibrational Raman scattering (VRS) in the ocean contributes significantly to the Ring effect. Chlorophyll and dissolved organic matter (DOM) absorb UV radiation in the ocean. This absorption decreases filling-in due to oceanic VRS. We examine the potential of using buv observations to determine chlorophyll and DOM content from the high-frequency spectral structure of earthshine spectra in clear conditions.

We briefly describe the GOME instrument in Section 2. The forward (radiative transfer) model and inverse (retrieval) model are described in sections 3 and 4, respectively. We provide error estimates from a linear analysis in 5. In section 6, we compare retrievals of cloud pressure from GOME with those from the collocated Along Track Scanning Radiometer-2 (ATSR-2). Conclusions and suggestions for future work are given in section 7.

2. GOME data

The GOME instrument was launched aboard the European Space Agency's (ESA) Second European Remote Sensing Satellite (ERS-2) in 1995 [*Burrows et al.*, 1999]. The ERS-2 is in a near-polar sun-synchonous orbit with a mean equator crossing time of 10:30 LST. Its mean altitude is 785 km.

GOME is a double monochromator that measures the the earthshine radiance and solar irradiance between 240 and 790 nm in four spectral channels. Solar irradiance measurements are made once per day. In this paper we use data from channel 2 that contains measurements in wavelength range 312-406 nm at a spectral resolution of 0.17 nm.

The nominal across-track swath width is 960 km and consists of 3 pixels that cover a ground area of 40 $\times$ 320 km. However, in this paper we use data in the small swath mode where the ground pixels are 40 $\times$ 80 km for a swath width of 240 km.

3. Forward Model

3.1. TOMRAD radiative transfer model

The normalized (by the incoming solar irradiance) backscattered intensity, I_R, observed at the top of the atmosphere can be expressed by

$$I_R = I_R(R = 0) + RI_g\gamma/(1 - RS_b), \quad (1)$$

where R is the surface reflectivity, I_g is the total radiance reaching the surface, γ is the transmittance of the radiance reflected from the surface, and S_b is the component of the reflected surface radiance that is scattered by the atmosphere back to the surface. Both I_g and γ can be separated into direct and diffuse components.

The forward model used here to compute these components at every iteration of scattering is similar to that used by *Joiner et al.* [1995] and is commonly referred to as TOMRAD. TOMRAD is an offspring (several generations removed) of work done originally by *Dave* [1964]. TOMRAD computes the source function at various vertical grid points in a vertically inhomogeneous atmosphere with molecular scattering and gaseous absorption using the straight forward successive orders of scattering method.

Polarization of the scattered light is modeled using a modification of the classic Rayleigh scattering phase matrix due to molecular anisotropy and Raman scattering [*Ahmad and Bhartia*, 1995]. Although no frequency redistribution of the Raman scattered energy is explicitly computed by TOMRAD, the successive order method allows for this to be approximated as done by *Joiner et al.* [1995]. The King correction factors computed by *Bates* [1984] are used to correct the Rayleigh (molecular) phase matrix.

Any number of absorbing gases can be included in the atmosphere and can have absorption coefficients that are quadratic with temperature, but only linear-type absorption is modeled. The lower reflecting surface is diffuse and follows Lambert's cosine law.

While Dave's original work was done for a plane-parallel atmosphere, TOMRAD has two modifications for a spherical atmosphere. Firstly, the direct solar beam is attenuated in a spherical atmosphere to the computational zenith. After this, the source function for each scattering event is computed in a plane-parallel atmosphere.

Secondly, the reflected intensity is calculated using the above computed source function in the integration of the source function method [*Kourganoff*, 1963] for a spherical atmosphere. For each satellite view angle plane-parallel source functions (with the spherical correction of the solar beam) are attenuated out of the atmosphere to the top of the at-

mosphere using scattering path lengths that are correct for a spherical atmosphere. These two corrections have been compared to results with a fully spherical model and have errors less than 0.1% for all view angles in plane 90° in azimuth to the solar plane and the nadir direction [*Caudill et al.*, 1997]. Larger errors on the order of 10% can occur for satellite view angles in the solar plane at a solar zenith angle of 88°.

3.2. Rotational-Raman scattering (RRS)

We compute RRS filling-in based on *Joiner et al.* [1995]. We updated the model by computing line strengths and frequencies shifts using D_o, the centrifugal distortion constant, that provides for more accuracy (D_o=5.76e-6 for N_2 and D_o=4.852e-6 for O_2). As in *Joiner et al.* [1995], we treat O_2 as a simple linear molecule which should be sufficient at the spectral resolution considered here [*Sioris*, 2001].

We extended the approach to off-nadir satellite observations. The only modification necessary is to compute the cosine of scattering angle of the single-scattered light (not encountering cloud or ground) as

$$cos(\Omega) = -cos(\theta_o) * cos(\theta) + sin(\theta_o) * sin(\theta) * cos(\phi), \quad (2)$$

where θ is the satellite zenith angle and ϕ is the azimuth angle difference between the solar and satellite zenith angles.

To analyze limitations of the RRS model of *Joiner et al.* [1995] and obtain insight into its basic assumptions, the model was reexamined with a more rigorous approach for its formulation. The radiative transfer equation for inelastic scattering *Vountas et al.* [1998] was solved using the straightforward successive orders of scattering method. It appeared

that a solution for the inelastic component of radiation can be expressed through the elastic component at every order of scattering only if certain assumptions are valid.

First, changes to the optical depth of the atmosphere and the single scattering albedo within the RRS band (*i.e.*, for wavelengths of RRS lines) should be small. This is true for Rayleigh scattering in the spectral range under consideration because the typical width of the RRS band is about 1 nm. However, this assumption may not be valid for wavelengths where ozone absorption changes abruptly within the spectral range of 1 nm.

For the first order of scattering the assumption of smooth atmospheric transmittance is the only assumption required for expessing the inelastic scattering through the solution for the elastic scattering. However, for higher orders of scattering an additional assumption is necessary; Namely, the RRS phase scattering function can be replaced by the Rayleigh phase scattering function. The assumption is corrected to some extent by introducing a correction factor which is the solid-angle average of the ratio of those phase scattering functions. The correction factor is fully consistent with the assumption of *Joiner et al.* [1995] that in scatterings of orders higher than one the scattering volume is illuminated from all directions by unpolarized light, and a fraction of the scattered light contained in the Cabannes line is replaced by its solid-angle average.

Another assumption is required in the rigorous formulation of the RRS model. The filling-in factor at every order of scattering is expressed through convolution of the elastic solution for the same order of scattering with the RRS spectrum. We replace this convolution by a convolution of the total elastic radiance with the RRS spectrum as it has been done in *Joiner et al.* [1995]. This procedure is supposed not to involve any significant error because the Fraunhofer line structure is preserved in elastic scatterings.

Finally, in *Joiner et al.* [1995], light that is Raman scattered more than once is neglected. This amounts to a small net loss of radiation. Accounting for this radiation is computationally expensive as it involves multiple convolutions. If instead, we assume that this energy is retained in the first-order-scattered Raman spectrum, we arrive at the relationship

$$\overline{k}_n = \frac{1-\overline{f}_o^n}{1-\overline{f}_o}\overline{k}_1, \tag{3}$$

where $\overline{k}_n$ is the filling-in factor for the nth order and $1-\overline{f}_o$ is the solid-angle average fraction of energy contained in a Raman lines in a single scattering. This is a reasonable approximation as a significant amount of the formerly lost energy is scattered back to the same wavelengths of the single-scattered Raman spectrum. This formulation presents a negligible difference in total filling-in with that computed using the relationship $\overline{k}_n = n\overline{k}_1$ in *Joiner et al.* [1995].

Figure 1 shows the dependence of the Ca K line filling-in on LER cloud (surface) pressure at GOME spectral resolution. The filling-in factor is defined by *Joiner et al.* [1995] as the percent difference between radiance computed with and without elastically scattered light. The RRS dependence on pressure is nearly linear for pressures greater than 0.4 hPa. Similarly, Figure 2 shows the reflectivity dependence of filling-in. The sharp decrease in RRS with increasing R at low θ_o and low values of R is related to an increase in the direct component of the radiance which does not undergo RRS. However, the filling-in begins to increase with R at about $R = 0.4$, where an increase in the scattered light between the surface and atmosphere (related to S_b) becomes important. The R dependence of the filling-in is important because it primarily determines how sensitive the cloud pressure retrieval will be to an error in absolute calibration as will be discussed later.

3.3. O_2-O_2 absorption in the ultraviolet

There are two relatively weak absorption lines of O_2-O_2 in the 350-400 nm wavelength range (360.4 nm and 380.2 nm). The O_2-O_2 absorption cross sections are taken from *Greenblatt et al.* [1990]. the vertical computational grid used in TOMRAD.

Figure 3 shows the fractional change in normalized radiance due to O_2-O_2 absorption at different surface pressures. The wiggles in the line center at low pressure are due to weak O_3 absorption. Figure 4 is similar to figure 1 but for O_2-O_2 absorption rather than RRS. Because of the pressure-squared dependence of the absorption, these curves are less linear than those for RRS. They also approach zero at higher pressures than RRS, so that the sensitivity to cloud pressure is relatively low at lower pressures.

To characterize the effect of O_2-O_2 absorption, we use a concept similar to the filling-in factor:

$$\delta = 1 - \frac{R(\lambda_m)}{[R(\lambda_m + \Delta\lambda) + R(\lambda_m - \Delta\lambda)]/2}, \tag{4}$$

where $R(\lambda_m)$ is normalized radiance at the core of an O_2-O_2 line (λ_m = 360 nm), and $R(\lambda_m \pm \Delta\lambda)$ is that in the line wings (*e.g.*, $\Delta\lambda$ = 10 nm), *i.e.*, beyond the absorption band.

Figure 5 shows the R dependence of O_2-O_2 absorption which is qualitatively different than that of RRS. The increase in R at low R increases O_2-O_2 absorption, whereas it decreases the fractional amount of observed Rayleigh scattering and thus decreases RRS.

3.4. Thin cloud simulations

Full Mie-scattering calculations in a cloudy atmosphere in the O_2-O_2 bands were performed using the University of Arizona Gauss-Seidel iteration code [*Herman and Brown-*

ing, 1965]. A similar model to compute the RRS filling-in under the same conditions has also been developed (to be described elsewhere [*Flittner and Joiner*, 2002]).

Clouds were assumed to be horizontally and vertically uniform. A C1 cloud model with a modified gamma size-distribution of water droplets was used [*Deirmendijan*, 1969]. Simulations were carried out for three cloud scenarios with physical cloud-top pressures of P_c=300, 500, and 700 hPa. Geometrical thickness of the clouds was defined by a constant pressure difference of 200 mb between the top and bottom cloud pressures. The simulations included aerosol scattering. A maritime aerosol model was assumed with the aerosol optical thickness of 0.15 at 550 nm. RRS was not included in the calculations.

Figure 6 shows O_2-O_2 absorption line depth versus the physical cloud top height for clouds with different optical depths at 360 nm. The O_2-O_2 absorption dependence on cloud optical depth (τ) saturates at about $\tau = 25$. An interesting effect is the response for the lowest cloud. It can be seen that there is enhanced absorption for the thick cloud as compared with the thin cloud or no cloud. This is the result of the reflectivity dependence of O_2-O_2 absorption that increases the photon path length between the ground and scattering atmosphere above.

Figure 6, similar to that shown for RRS by *de Beek et al.* [2001], illustrates the increase in photon path and thus O_2-O_2 absorption with decreasing τ. For example, a $\tau = 5.0$ cloud at 8 km produces the same amount of O_2-O_2 absorption as a $\tau = 20$ cloud at 5 km.

Simulations were performed with the thin cloud RRS model for a 100 hPa thick cloud at several cloud top pressures between 400 and 900 hPa at $\theta_o = 55°$ and for $\tau = 0.1 - 50$. The simulations showed that the retrieved LER cloud pressure would be about 50-80 hPa

higher than the physical cloud top for $\tau > 2$. These results are similar to the findings of *de Beek et al.* [2001].

3.5. Ocean Raman effects

Vibrational Raman scattering in the ocean contributes significantly to the Ring effect [*e.g., Kattawar and Xu*, 1992] and has been observed in buv observations [*Vasilkov et al.* 2002]. A radiative transfer model for ocean filling-in has been developed by *Vasilkov et al.* [2002] and compared with GOME observations at the Ca K line. The model was able to simulate the observed excess filling-in in clear waters and decreased filling-in over turbid waters using climatological values of chlorophyll content. However, there still remains some uncertainty in the pure water absorption at these wavelengths. The spectral and solar zenith angle dependence of the ocean filling-in is different from that of atmospheric RRS. Therefore, it may be possible to retrieve an effective scene pressure independently of chlorophyll content.

Figure 7 shows the spectral dependence of the filling in, calculated at GOME resolution, due to both atmospheric and oceanic Raman scattering. For shorter wavelengths, the ocean filling-in is negative representing a net depletion of energy due to the dominance of energy transfer from those wavelengths to longer wavelengths over the energy gain from shorter wavelengths. The spectral signature is similar for atmospheric and oceanic filling-in. However, the magnitude of the oceanic filling-in decreases with wavelength owing to reducing amounts of radiation reaching the surface at excitation wavelengths in the ozone Huggins bands.

3.6. Table generation

Tables of the iteration values output from the TOMRAD code were generated for wavelengths between 340 and 400 nm for a single O_3 profile (because O_3 absorption is very weak in this spectral range, a single profile will suffice) for 5 difference surface pressures, 10 solar zenith angles, 6 satellite zenith angles, and 7 azimuth angles. Using a GOME solar spectrum, a second set of tables of the RRS filling-in and normalized radiance for these geometries were generated at GOME spectral resolution for 6 seflectivities. A table for the ocean filling-in was created using the *Vasilkov et al.* [2002] model for the same geometries and reflectivities. These tables will be used to compute radiances by linear interpolation in the next section for the retrieval of cloud pressure.

4. Inverse Model

The general approach for retrieving the LER cloud pressure (CP) is a minimum variance algorithm based on table lookup. The details are described in this section.

4.1. Reflectivity calculation

The Lambertian-equivalent reflectivity, R, is calculated at 373.2 nm by inversion of (1). This wavelength was chosen such that it is relatively free of RRS and O_2-O_2 absorption.

4.2. Cloud pressure retrieval by least-squares fitting

The cloud pressure is retrieved by an iterative minimum-variance (least-squares) solution of the form

$$x_{n+1} = x_n + (H'(W)^{-1}H)^{-1}H'(W)^{-1}(y_{\text{obs}} - y_{\text{calc}}), \tag{5}$$

where x_n is state vector estimate at iteration n, H is the Jacobian matrix (partial derivatives of the observation vector with respect to the state vector), W is the observation error

covariance which includes measurement and forward model error, and y_{obs} and y_{calc} are vectors of observed and calculated radiances, respectively. The retrieval error covariance, E, is then given by

$$E = (H'(W)^{-1}H)^{-1}. \quad (6)$$

The observation vector includes normalized radiances from 355-400 nm or a subset of wavelengths in that spectral range. The observations are spline-interpolated to the table wavelengths which have a 0.2 nm spacing. This greatly reduces the amount of computation required for interpolation. The observation error covariance, W, is a diagonal matrix with the square root of the diagonal set conservatively to 1% of the observed value.

The state vector includes three coefficients to form a quadratic fit of the low-frequency component of the radiances (*i.e.*, $A+B\lambda+C\lambda^2$), two coefficients to correct for wavelength differences between the solar irradiance and earth-view spectra (shift and squeeze), and the cloud pressure. The quadratic coefficients account for Rayleigh scattering as well as calibration errors so that the cloud pressure is determined only from the high-frequency component of the spectra. Over ocean or large lakes, chlorophyll content (CHL) can be added to the state vector.

The magnitudes of the wavelength shift, $(\Delta\lambda)$, and squeeze, $(\hat{\lambda})$, are assumed to be constant over the given spectral interval. Therefore, the spectrally shifted and squeezed quantities are calculated as $f(\lambda + \Delta\lambda)$ and $f(\hat{\lambda}\lambda)$ respectively. It is the shift and squeeze coefficients that contribute to nonlinearity and necessitate an iterative solution.

The radiances y_{calc} are computed by linear interpolation of the tables in R, θ_o, θ, ϕ, and pressure P. The pressure, chlorophyll, and wavelength shift and squeeze Jacobians are computed by finite differences. For clear ($R < 15\%$) and overcast ($R > 40\%$) pixels, all

calculations are performed at the retrieved value of R. Mixed scenes ($0 <$ cloud fraction < 1) will not be considered here.

At every iteration a quantity χ is computed, defined by

$$\chi = ([y_{\text{resid}}]W^{-1}[y_{\text{resid}}]')^{0.5}/N, \tag{7}$$

where N is the number of observations and y_{resid}, called the radiance residual, is defined as $y_{\text{resid}} = y_{\text{obs}} - y_{\text{calc}}$. Iterations continue until $(\chi_{n-1} - \chi_n)/\chi_{n-1} < 0.03$. The pixel is flagged if convergence does not occur within 6 iterations. The algorithm typically converges in 3 iterations.

5. Sensitivity analysis

5.1. Error estimates due to random instrument noise

Using (6), we can estimate the errors in retrieved parameters. This linear error estimate is computed at the final iteration of the retrieval process, minimizing effects of non-linearity. The estimate assumes that observation biases and spectrally-correlated errors are negligible. As shown in the next section, these assumptions are not met, so that is not an absolute error estimate. However, the analysis gives an estimate of the error due to random instrument noise and provides some insight on the errors correlations in the retrieved parameters.

The error estimate is unique for every situation, because the Jacobian depends upon the satellite geometry, reflectivity, and the number of retrieved parameters. Table 1 gives some sample values of error standard devations (σ) for LER cloud pressure (P), wavelength shift ($\Delta\lambda$), wavelength squeeze($\hat{\lambda}$), and chlorophyll concentration (CHL) along with the retrieved CHL, the solar zenith angle (θ_o), reflectivity (R), and the correlation between

P and CHL errors ($c_{P,CHL}$). The values in Table 1 are calculated assuming a Gaussian observation error with $\sigma = 1\%$.

Typically, for a fully cloudy pixel with high reflectivity, the estimated error in LER cloud pressure is ~25hPa. If chlorophyll is not included in the state vector, the error correlations are all less than 10%. This indicates that the retrieved parameters are more-or-less unique. For clear conditions (low reflectivity), the cloud (surface) pressure errors nearly double to about 50hPa while the correlations remain at less than 10%. The wavelength shift and squeeze errors are always low and are virtually uncorrelated with the other parameters. This is because the spectral structure induced by these parameters is nearly orthogonal to that produced by the others, including cloud pressure.

When chlorophyll is added to the state vector under clear conditions, the pressure error doubles approximately to about 120 hPa, but this error is highly correlated with the chlorophyll error (93%). Therefore, P and CHL cannot be uniquely determined within the given standard deviation ranges. The CHL error depends upon the retrieved value of CHL. The error is higher, both in absolute amount and percentage, for higher values of chlorophyll. This is because the sensitivity begins to saturate at higher values of CHL where the contribution of vibrational Raman scattering in the ocean becomes negligible [see *Vasilkov et al, 2002*]. In these samples, CHL errors range from approximately 60% at CHL=0.42 to about 35% at CHL=0.094.

5.2. Sensitivity to absolute calibration error

Because P and CHL are determined from the high-frequency spectral structure from RRS and O_2-O_2 absorption, errors in absolute calibration factor in only through the determination of R. RRS varies strongly with R at low R and weakly with R at high

R. Therefore, in overcast conditions, the retrieval of P will be relatively insensitive to absolute calibration.

For example, a 10% error in absolute calibration (Earth radiance with respect to solar flux) will produce a change of about 10% in R. The resulting change in P is only about 20-30 hPa. However, at low R, a 10% calibration error may change R by only about 3%, but this will produce a change in P of about 100 hPa.

6. Results and Comparisons With other Data

6.1. Cloud pressure comparison with ATSR-2

The retrieved CP can be compared with that derived from thermal infrared observations from the Along Track Scanning Radiometer-2 (ATSR-2). ATSR-2 also flies on ERS-2 and produces visible and infrared images of the Earth in 7 channels at a spatial resolution of 1 km. A data set of ATSR-2 cloud-top pressure and fraction has been produced where ATSR-2 pixels are collocated with the GOME small pixels and averaged over the same ground footprint. Here we focus on GOME pixels for which $R > 40\%$ and the retrieved ATSR cloud fraction was 100% thus indicating relatively thick cloud covering a majority of the pixel.

Figure 8 shows the ground path of GOME orbit 80324174 (orbit 174 from March 24, 1998). This orbit has a good sample of cloud free pixels over ocean where chlorophyll content varies from very high values near the North American coast to very low in the Pacific desert. There are overcast conditions at high latitudes in both hemispheres and also near the equator.

Figure 9 shows a comparison of the retrieved cloud pressures from GOME and collocated ATSR-2. GOME LER cloud pressures were higher than IR ATSR by an average of about

180 hPa and the standard deviation is approximately 100 hPa. Figure 10 is a scatter diagram of the cloud pressures obtained using GOME and ATSR. The correlation is 0.75 and was as high as 0.80 for other orbits. Figure 9 shows that the scatter is not completely random in nature. There appear to be several types of cloud that have varying magnitudes of the UV-IR differences. For example, the pixels between 65 and 70°S have a significantly smaller difference than those between 65 and 70°N. These systematic differences are much greater than the expected error due to random noise.

The correlation is best for the equatorial region where high optically thick clouds are observed. It is reasonable to suppose they are nimbostratus or of the deep convection type. The correlation is also high for the geographical region between 40 and 60°S. Most clouds in the region have moderate optical depths ($R < 60\%$). The correlation is smaller for the northern region between 40 and 75°N. Most clouds in this region are optically thick ($R > 0.7$). It is possible that enhanced scattering between cloud and a snow/ice-covered surface or a secondary cloud deck increases the retrieved LER pressure, producing a significant difference with the IR cloud pressures.

The correlation and standard deviation are better than was obtained by JB95 with TOMS/SBUV THIR for $R > 40\%$, most likely due to the higher signal-to-noise ratio of GOME. The IR/UV bias is of the same sign, however slightly larger than JB95. Similar statistics are obtained for other orbits. Significantly higher cloud pressures derived from the GOME oxygen-A band as compared with ATSR-2 were also reported by *Koelemeijer and Stammes*, 2000]. They used a similar modified LER approach where cloud fractions were derived along with cloud pressures. The GOME/ATSR-2 differences were most pronounced for optically thick cloud where the derived cloud fractions were close to one.

Because their GOME cloud pressures were derived from absorption at visible wavelengths, their GOME/ATSR-2 differences should be and are similar to ours.

There was no obvious dependence of the IR/UV difference on R (which is related to cloud optical thickness) or θ_o. This leaves open the possibility that the differences may be related to other cloud geometrical parameters such as the physical thickness. Simulations with the thin cloud RRS and O_2-O_2 models have shown that for the same COT and physical cloud top pressure (hence the same R), increasing the vertical thickness of the cloud increases the filling-in. This in turn causes the LER retrieved CP to be larger. In addition, increases in the filling-in due to increased vertical thickness increase with COT. However, the observed IR/UV differences are sometime significantly larger than those expected from even a very thick cloud. Multiple cloud decks may explain these large differences.

6.2. Retrieval of surface pressure and chlorophyll over clear pixels

In order to evaluate the ocean Raman model as well as the cloud pressure retrieval algorithm, we performed retrievals over cloud-free ($R < 15\%$) pixels. Several different methods were tested to retrieve the scene pressure over ocean: (1) No ocean Raman scattering is included in the radiative transfer calculations with (a) All wavelengths 355-400 nm (b) Only 355-360 nm where the effects of ocean Raman scattering are small. (2) Ocean Raman scattering is included using climatological values of chlorophyll absorption. (3) Chlorophyll is treated as an additional state variable within the retrieval algorithm.

Figure 11 shows retrieved surface pressures over clear ocean scenes for GOME orbit 80324174 where the expected P is $\sim$1.0. Not accounting for ocean Raman scattering leads to significant errors in the retrieved scene pressure. Restricting the retrieval algo-

rithm to use only shorter wavelengths less affected by ocean Raman scattering improves the retrievals, but still leaves significant errors. The use of climatological chlorophyll further reduces but does not eliminate errors in the retrieved scene pressure. The remaining error could result from the actual chlorophyll deviating from the climatological values used here or errors in the ocean radiative transfer model including the UV optical parameters. Allowing chlorophyll to be an additional state variable in the algorithm significantly improves the retrieval of surface pressure with small errors still remaining especially in clear ocean water.

Figure 12 shows the retrieved chlorophyll concentration and for comparison, the annual mean climatological values that were used as a first guess, and weekly data from SeaWIFS [`http://seawifs.gsfc.nasa.gov/SEAWIFS.html}]`.Similar spatial variations in chlorophyll are retrieved using VBS, including very low values in the southern Pacific and higher values approaching the North American coast. This initial comparison is very promising considering the relatively large GOME footprint and uncertainties in water optical properties.

6.3. Radiance residuals

Figure 13 shows y_{resid} (at convergence) for several different GOME pixels. Residuals are generally small in the range $\pm 0.5\%$ which is comparable to those shown for lower spectral resolution instruments in *Joiner et al.* [1995]. The residuals are similar in all pixels. Thus, the forward model and/or observation errors have significant correlation. The uncorrelated component (standard deviations) are low (0.2%), indicating that the signal-to-noise ratio of the GOME instrument is extremely high at these wavelengths.

For the high latitude cloudy case (high R) where the solar zenith angle is high, residuals are higher in the vicinity of the O_2-O_2 bands. This could indicate that the LER approximation produces some error. Alternatively, there may be an error in the O_2-O_2 cross sections, in our RRS forward model, or in the observations (*e.g.*, unmodeled polarization sensitivity).

Our thin cloud simulations show that absorption due to O_2-O_2 in and below the cloud affects radiances differently than excess Rayleigh/Raman scattering. Because more wavelengths are affected by RRS and the RRS signal is larger, the algorithm fits the RRS part of the spectrum and a residual remains in the O_2-O_2 bands.

The residuals in the O_2-O_2 bands are smaller in the mid-latitude cloudy spectrum. One explanation is that the LER model works better for this pixel. The solar zenith angle is also smaller, which could decrease the effects of non-LER behavior. This effect could also be consistent with an error in the O_2-O_2 cross sections as the residual in this case would decrease with photon pathlength (solar zenith angle).

Residuals are slightly smaller in the clear pixel (low R) which is expected as the surface should be more Lambertian. In addition, the low reflectivity decreases absorption due to O_2-O_2 and would therefore decrease the residual due to a cross section error.

For the high equatorial cloud, residuals in the O_2-O_2 band are relatively small. In this case, O_2-O_2 absorption is generally smaller due to the high cloud. The LER model appears to be adequate to fit the radiance spectrum.

There are several potential sources of bias including polarization effects. GOME is known to have polarization sensitivity. A correction is applied to the spectra used here, but that correction is a relatively smooth function of wavelength. It therefore does not account

for higher frequency errors that would be associated with the polarization sensitivity of rotational-Raman scattering described in *Kattawar et al.* [1981] and observed by *Solomon et al.* [1987].

Polarization should affect low reflectivity pixels more than high reflectivity (cloudy) pixels. To verify this, we retrieved pressure over clear land pixels. The retrieved pressures were systematically lower than the climatological pressure by 200 hPa. The pixels were screened for aerosol contamination. This bias could be due to a combination of absolute calibration error and polarization sensitivity, both of which may have a significant effect on low reflectivity pixels, but a much smaller effect on high reflectivity scenes. Note that this low-pressure bias is of the opposite sign of the UV-IR bias.

There are also indications that in some GOME spectra a single squeeze and squeeze combination is not adequate to describe wavelength differences between Earth and solar observations. We note that these spectra with higher residuals occur systematically near the same latitudes in every orbit we examined. This could be linked to temperature changes on the satellite due to solar heating and/or other instruments being turned on/off. The residuals tend to increase at high southern latitudes.

7. Conclusions and Future Work

We have shown that cloud pressure can be retrieved using buv measurements throughout the spectral range between 355 and 400 nm. Comparisons with coincident IR-dervied cloud pressure show that UV-derived LER cloud pressures are higher. Simulated radiances in thin cloud indicate that light penetrating the cloud causing absorption by O_2-O_2 and enhanced RRS from Rayleigh scattering should indeed result in a LER pressure higher

than the physical cloud top. In addition, excess scattering from multiple-layer clouds will also increase LER cloud pressures.

We also showed that the retrieved scene pressure over clear ocean improves when chlorophyll content is added to the state vector. Initial comparison of retrieved chlorophyll with that derived from SeaWIFS shows that vibrational Raman scattering is a promising new techique for deriving information about chlorophyll and other UV-absorbing matter in water. The approach has high sensitivity in relatively clear waters (low chlorophyll levels) and a relatively small sensitivity to errors in absolute calibration and other atmospheric effects such as Rayleigh scattering. We plan to investigate the sensitivity of retrieved chlorophyll and possibly dissolved organic matter to optical parameters and other aspects of the ocean radiative transfer model.

This paper focused on thick cloud covering the majority of a GOME pixel. These are the situations of maximum impact on O_3 retrievals and of the most interest for retrieving tropospheric O_3. We plan to extend this work to partially cloudy cases. However, complications will arise when intercomparing data sets from different instruments due to differences in the pixel size and thus the implied cloud fraction, especially in the presence of thin partial cloud.

The cloud pressure retrieval algorithm presented here is being developed in part for use with the Ozone Monitoring Instrument (OMI) that will fly on the National Aeronautical Space Administration (NASA) Earth Observing System (EOS) Aura satellite. OMI will have a significantly smaller footprint (12 $\times$ 24 km) than GOME with a larger swath, similar spectral coverage and somewhat lower spectral resolution [*Stammes et al.*, 1999].

EOS-Aura will fly in formation with several other satellites carrying instruments designed to measure cloud properties including the VIS/IR imager Moderate Resolution Imaging Spectroradiometer (MODIS) on EOS-Aqua, a dual wavelength lidar and infrared imager on Cloud-Aerosol Lidar and Infrared Pathfinder Satellite Observations (CALIPSO), and a 94 GHz radar on CloudSat. These instruments will make measurements over the same area within 20 minutes of OMI. We plan to examine the information content of a multi-spectral approach using passive UV, VIS, and IR observations for retrieving information about cloud vertical extent and the existence of multiple cloud decks. It is hoped that the active sensors in this satellite formation can be used to evaluate the concept.

Acknowledgments. This work was supported in part by NASA under the algorithm development program for the Earth Observing System Aura Ozone Monitoring Instrument (EOS Aura OMI). The authors thank the European Space Agency (ESA), the UK Natural Environment Research Council, and the Rutherford Appleton Laboratory for their support in supplying ATSR-2 data and ESA for providing the GOME level 1 data. We also thank Piet Stammes, Johan de Haan, and Juan Accareta for helpful comments.

References

Ahmad, Z. and P. K. Bhartia, Effect of molecular anisotropy on the backscattered UV radiance. *Appl. Opt.*, *34*, 8309–8314, 1995.

Bates, D. R., Rayleigh scattering by air. *Planet. Space Sci.*, *32*, 785–790, 1984.

de Beek R., Vountas, M., Rozanov, V. V., Richter, A., and J. P. Burrows, The ring effect in the cloudy atmosphere. *Geophys. Res. Let.*, *28*, 721–724, 2001.

Burrows, J. P. *et al.*, The Global Ozone Monitoring Experiment (GOME): Mission concept and first scientific results. *J. Atmos. Sci.*, *56*, 151–171, 1999.

Caudill, T. R., Flittner, D. E., Herman, B. M., Torres, O., and R. D. McPeters, Evaluation of the pseudo-spherical approximation for backscattered ultraviolet radiances and ozone retrieval. *J. Geophys. Res.*, *102,* 3881–3890, 1997.

Chance, K. V. and R. D. Spurr, Ring effect studies: Rayleigh scattering, including molecular parameters for rotational Raman scattering, and the Fraunhofer spectrum. *Appl. Op.*, *36*, 5224–5230, 1997.

Chandra S., Ziemke J. R., Min W., and W. G. Read, Effects of 1997-1998 El Nino on tropospheric ozone and water vapor. *Geophys. Res. Let.*, *25*, 3867–3870, 1998.

Chandra S., Ziemke J. R., and R. W. Stewart, An 11-year solar cycle in tropospheric ozone from TOMS measurements. *Geophys. Res. Let.*, *26*, 185–188, 1999.

Dave, J. V., Meaning of successive iteration of the auxiliary equation in the theory of radiative transfer. *Astrophys. J.*, *140*, 1292–1303, 1964.

Deirmendjian, D., Electromagnetic scattering on spherical polydispersions. American Elsevier Pub. Co., N. Y., N. Y., USA, 290 pp., 1969.

Flittner, D.E. and J. Joiner (2002): Atmospheric rotational Raman scatter spectrum as affected by aerosols/clouds: Nonabsorbing aerosols over dark surfaces, *to be submitted to Appl. Opt.*.

Grainger, J. F., and J. Ring, Anomalous Fraunhofer line profiles. *Nature*, *193*, 762, 1962.

Greenblatt, G. D., Orlando, J. J., Burkholder, J. B., and A. R. Ravishankara, Absorption measurements of oxygen between 330 and 1140 nm. *J. Geophys. Res.95*, 18577-18582, 1990.

Hsu, N. C., McPeters, R. D., Seftor, C. J., and A. M. Thompson, Effect of an improved cloud climatology on the total ozone mapping spectrometer total ozone retrieval. *J. Geophys. Res.102*, 4247–4255, 1997.

Hudson, R. D., Kim, J.-H., and A. M. Hudson, On the derivation of tropospheric column ozone from radiances measured by the total ozone mapping spectrometer. *J. Geophys. Res.100*, 11137–11145, 1995.

Joiner J., Bhartia, P. K., Cebula, R. P., Hilsenrath, E., and R. D. McPeters, Rotational-Raman scattering (Ring effect) in satellite backscatter ultraviolet measurements. *Appl. Opt.*, 1995.

Joiner J., and P. K. Bhartia, The determination of cloud pressures from rotational-Raman scattering in satellite backscatter ultraviolet measurements. *J. Geophys. Res.*, *100*, 23019-23026, 1995.

Kattawar, G. W., Young, A. T., and T. J. Humphreys, Inelastic scattering in planetary atmospheres. I. The Ring effect, without aerosols. *Astrophys. J. 243*, 1049-1057, 1981.

Kattawar, G. W., and X. Xu, Filling in of Fraunhofer lines in the ocean by Raman scattering. *Appl. Opt.*, *31*, 6491–6500, 1992.

Koelemeijer, R. B. A., and P. Stammes, Effects of clouds on ozone column retrieval from GOME UC measurements. *J. Geophys. Res.*, *104*, 8281–8294, 1999.

Koelemeijer, R. B. A., and P. Stammes, Comparison of cloud retrievals from GOME and ATSR-2, *Earth Obs. Quart., 65*, ESA publication ISSN 0256-5gbx, 25-27, 2000.

Koelemeijer, R. B. A., Stammes, P., Hovenier J. W., and J. F. de Haan, A fast method for retrieval of cloud parameters using oxygen A band measurements from the Global Ozone Monitoring Experiment. *J. Geophys. Res.106*, 3475-3490, 2001.

Kourganoff, V, Basic methods in transfer problems. Dover Publications, Inc. New York, 281 pp., 1963.

McPeters R. D., S. M. Hollandsworth, L. E. Flynn, J. R. Herman, and C. J. Seftor, Long-term ozone trends derived from the 16-year combined Nimbus 7 Meteor 3 TOMS Version 7 record. *Geophys. Res. Let.*, *23*, 3699–3702, 1996.

Ramanathan, V., The role of Earth radiation budget studies in climate and general circulation research. *J. Geophys. Res.*, *92*, 4075-4095, 1987.

Rossow, W. B., and R. A. Schiffer, ISCCP cloud data products, *Bull. Am. Meteorol. Soc.*, *72*, 2-20, 1991.

Sioris, C. E., Filling in of absorption lines in sky spectra due to rotational Raman scattering. PhD thesis, York University, Canada, 133 pp., 2001.

Solomon, S., Schmeltekopf, A. L., and R. W. Sanders, On the interpretation of zenith sky absorption measurements, *J. Geophys. Res. 92*, 8311-8319, 1987.

Stammes, P., Levelt, P., de Vries, J., Visser, H., Kruizinga, B., Smorenburg, C., Leppelmeier, G., and E. Hilsenrath, Scientific requirements and optical design of the Ozone Monitoring Instrument on EOS-CHEM. *Proc. SPIE Conf. on Earth Obs. Sys. IV, Denver, Co., USA, SPIE Vol. 3750*, 221–232, 1999.

Thompson, A. M., D. P. McNamara, K. E. Pickering, and R. D. McPeters, Effect of marine stratocumulus on TOMS ozone, *J. Geophys. Res.*, *98*, 23051–23057, 1993.

Vasilkov, A., Joiner, J., Gleason, J. F., and P. K. Bhartia, Ocean Raman scattering in satellite backscatter ultraviolet measurements. *Geophys. Res. Let.*, in press, 2002.

Vountas M., Rozanov V. V., J. P. Burrows, Ring effect: Impact of rotational Raman scattering on radiative transfer in Earth's atmosphere. *J. Quant. Spect. Rad. Trans.*,

60, 943-961, 1998.

Ziemke J. R., and S. Chandra, Seasonal and interannual variabilities in tropical tropospheric ozone. *J. Geophys. Res.*, *104*, 21425-21442, 1999.

Ziemke J. R., Chandra S., and P. K. Bhartia, "Cloud slicing": A new technique to derive upper tropospheric ozone from satellite measurements. *J. Geophys. Res.*, *106*, 9853–9867, 2001.

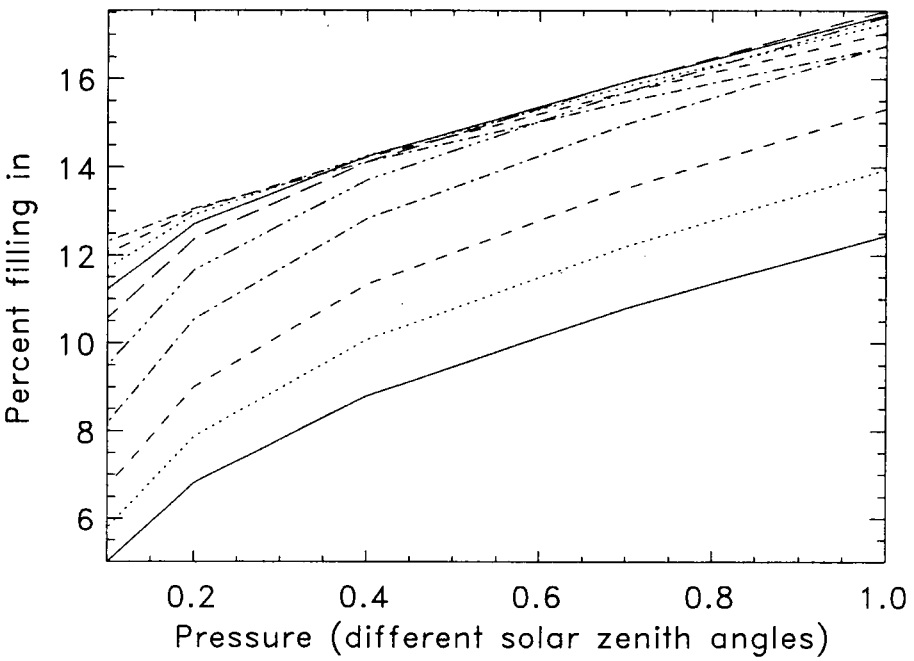

Figure 1. Filling-in at Ca K line as a function of pressure for different θ_o from 0 (bottom solid line), 30, 45, 60, 70, 77, 81, 84, 86, and 88° at $R = 65\%$ and $\theta = 15°$.

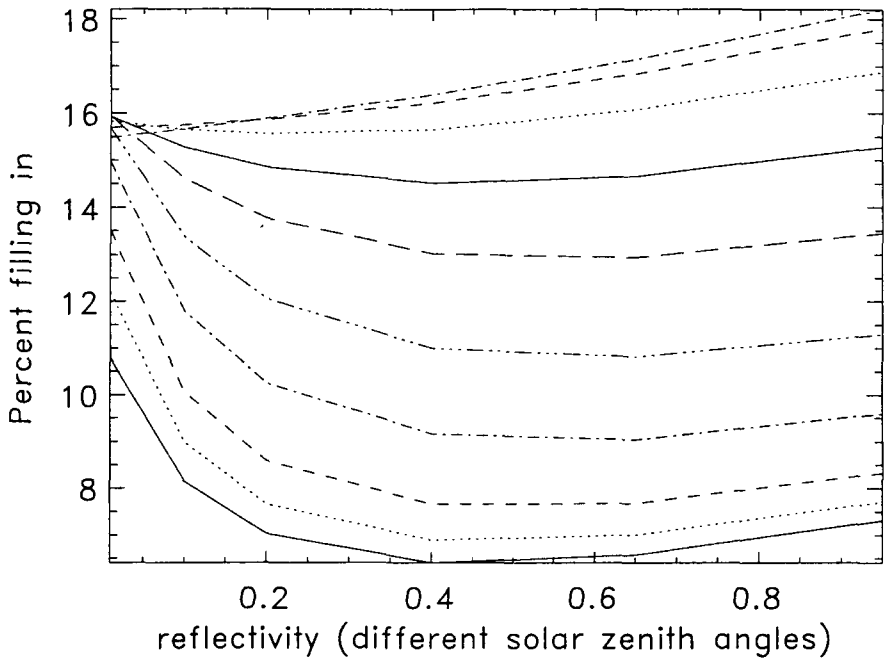

Figure 2. Similar to figure 1 but with R as the abcissa, compute at pressure 0.7 atm.

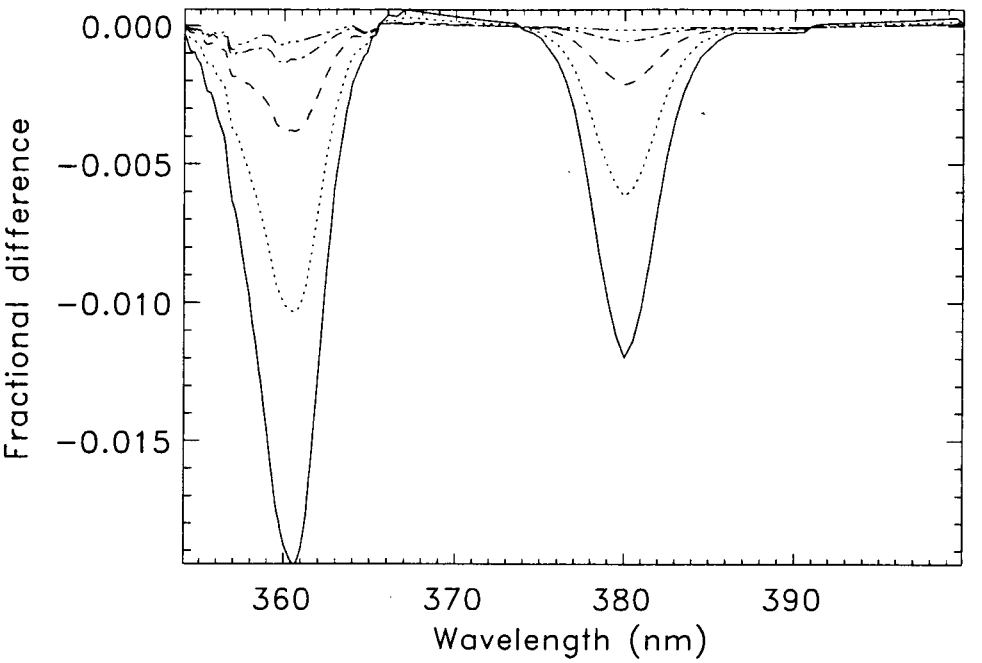

Figure 3. Fractional change in radiance due to $O_2 - O_2$ absorption at surface pressures 1013 (solid), 709 (dotted), 405 (dashed), 203 (etc.), and 101 hPa.

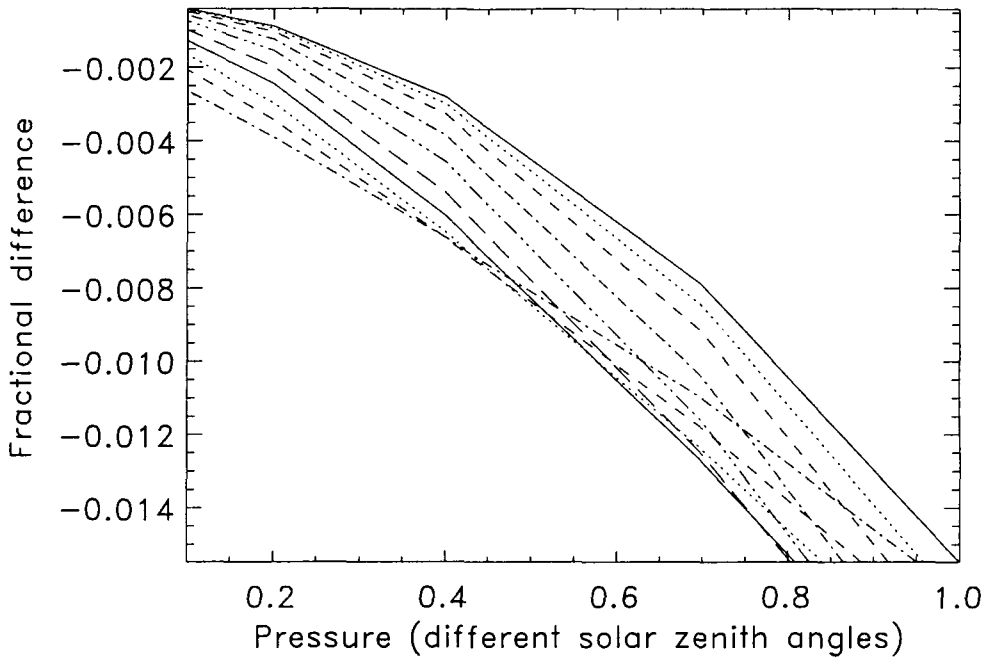

Figure 4. Fractional change in radiance at center of $O_2 - O_2$ line as a function of cloud pressure for difference solar zenith angles from 0 to 88°.

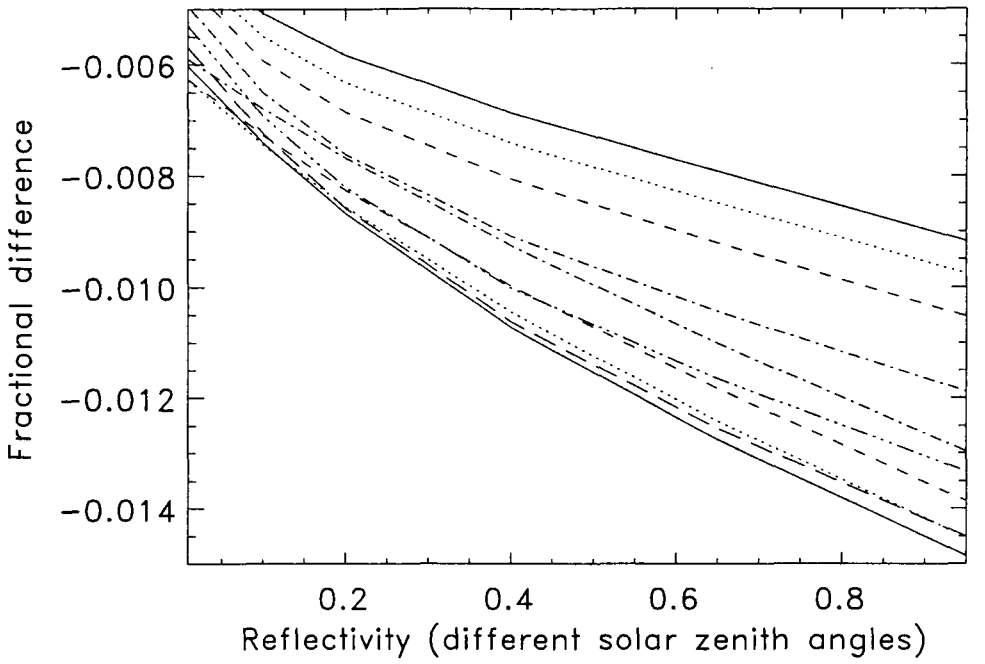

Figure 5. Similar to figure 2 but for $O_2 - O_2$ absorption.

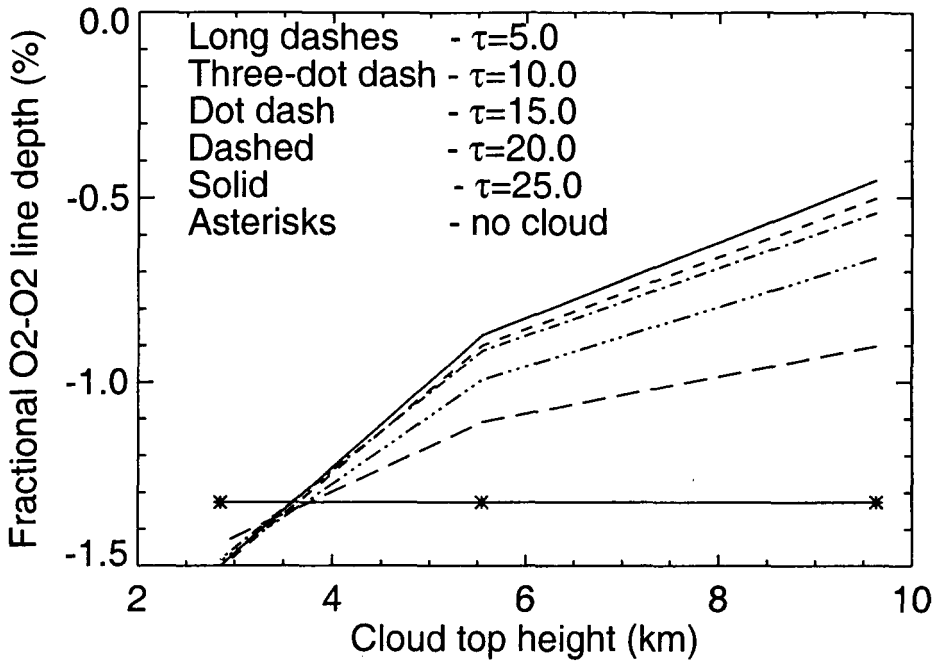

Figure 6. O_2-O_2 absorption dependence on cloud-top height and cloud optical depth for O_2-O_2 at 360 nm $\theta_o = 45°$, $\theta = 0°$.

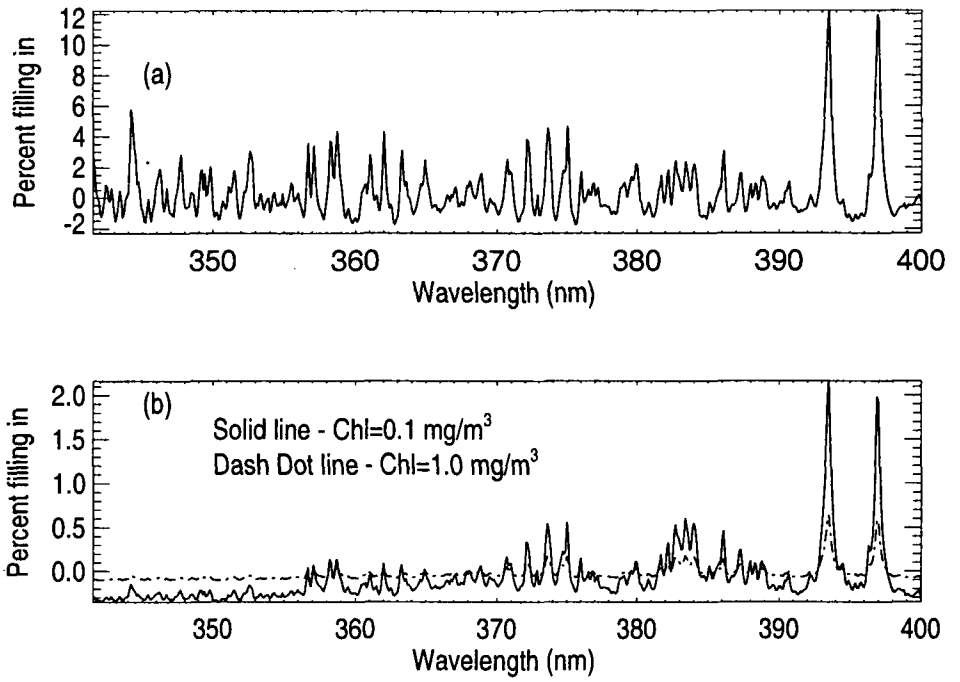

Figure 7. (a) Atmospheric Raman filling-in; (b) oceanic Raman filling-in for two chlorophyll concentrations, $R = 10\%$, $\theta_o = 45°$, nadir

Table 1. Errors (standard deviation) from linear estimate. (N/A indicates situation where oceanic quantities are not retrieved over land)

θ_o	$R(\%)$	σ_P (hPa)	$\sigma_\Delta\lambda$(nm)	$\sigma_{\lambda Sq}$	$\sigma_C HL$ (mg/m^3)	CHL(mg/m^3)	$c_{P,CHL}$ (%)
84.7	83.1	26	6.9e-4	2.8e-4	N/A	N/A	N/A
50.1	83.4	24	6.7e-4	2.7e-4	N/A	N/A	N/A
41.5	5.0	46	6.7e-4	2.7e-4	N/A	N/A	N/A
26.5	6.2	128	6.7e-4	2.7e-4	0.256	0.423	93
24.3	8.9	117	6.8e-4	2.7e-4	0.086	0.176	93
33.4	9.3	111	6.8e-4	2.7e-4	0.033	0.094	93

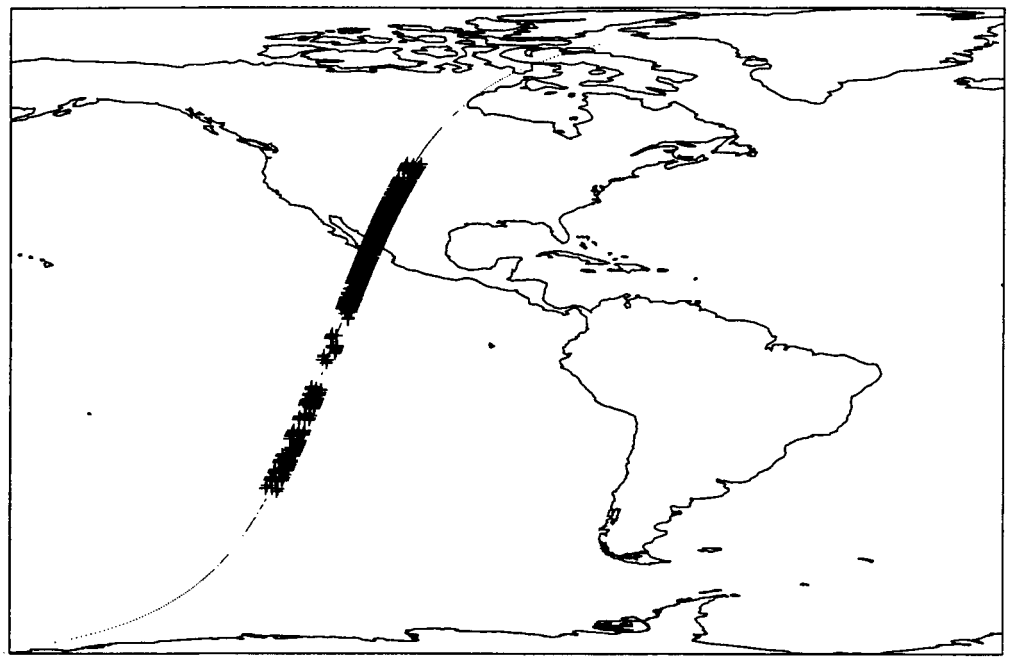

Figure 8. GOME orbit 80324174; Dots: Cloudy pixels ($R > 40\%$), +: Clear pixels($R < 15\%$)

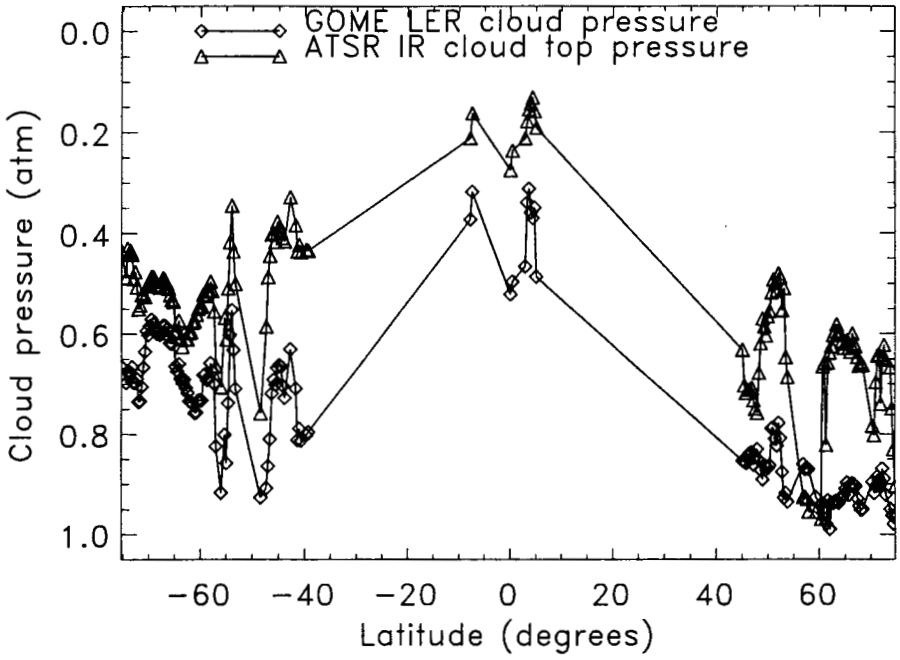

Figure 9. Comparison of retrieved cloud pressures.

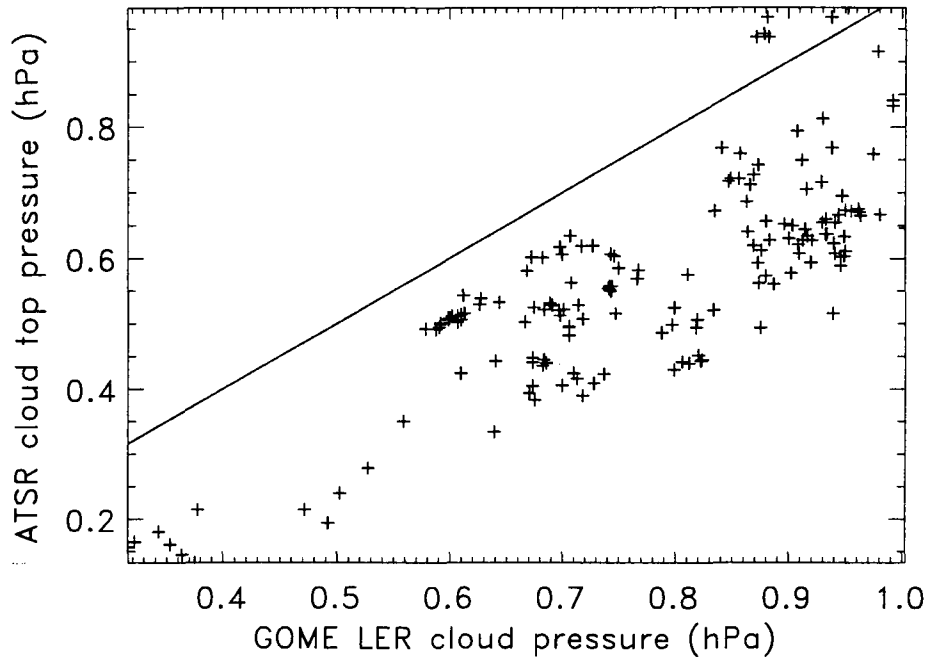

Figure 10. Scatter diagram of retrieved cloud pressures.

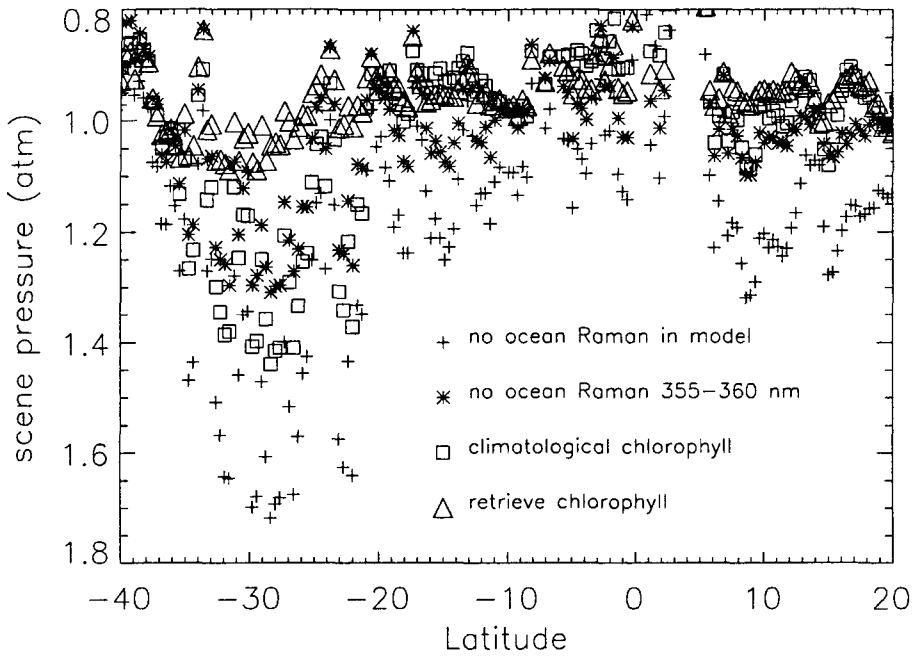

Figure 11. Retrieved surface pressure over clear ocean using different methods described in text.

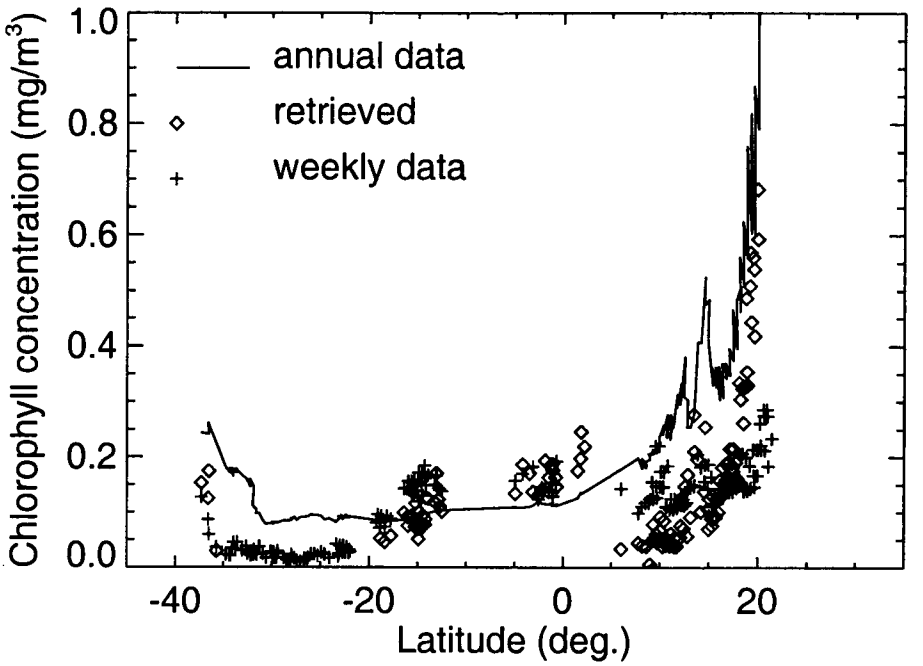

Figure 12. Retrieved chlorophyll and annual-mean and weekly values from SeaWIFS.

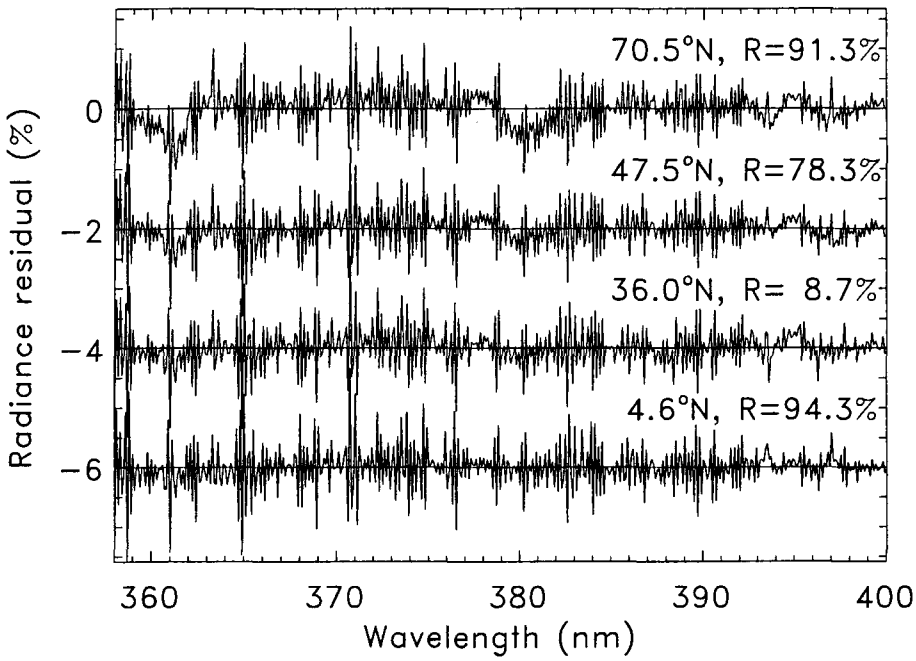

Figure 13. Radiance residual spectra from four different GOME pixels, offset for clarity. The latitude and reflectivity are given above.

accepted